FEATURE ARTICLE

The New Wave in Shock Waves

Dana D. Dlott,* Selezion Hambir, and Jens Franken

Box 01-6 CLSB, School of Chemical Sciences, University of Illinois at Urbana−Champaign, 600 S. Mathews Ave., Urbana, Illinois 61801

Received: October 21, 1997; In Final Form: January 7, 1998

Laser-driven shock waves (0−5 GPa) can be generated at high repetition rates (100/s) using a moderate-energy tabletop picosecond laser system and a multilayered microfabricated shock target array. High spatial resolution is needed to obtain high temporal resolution of the effects of a steeply rising shock front on molecular materials. The needed spatial resolution is obtained using a sandwich arrangement with a thin layer of sample material termed an "optical nanogauge". Experiments with an anthracene nanogauge show that ultrafast vibrational spectroscopy can be used to determine the shock temperature, pressure, velocity, and shock front rise time. Shock pulses can be generated with rise times <25 ps, which generate irreversible shock compression, and with rise times of a few hundred picoseconds, which generate reversible compression. These pulses, which have a duration of a few nanoseconds, are termed "nanoshock" pulses. Nanoshock pulses produce large-amplitude mechanical perturbations and can initiate and turn off thermochemical reactions, produce highly excited vibrational populations, and heat and cool condensed matter systems at tremendous rates. These applications are illustrated briefly in nanoshock experiments on an energetic material and a heme protein. Using high repetition rate nanoshocks to study large-amplitude molecular dynamics in molecular materials important in chemistry and biology is the new wave in shock waves.

1. Introduction

Shock waves in condensed matter provide a way of very rapidly attaining extreme conditions of high pressure, high density, and high temperature.[1,2] With shock compression it becomes possible to suddenly turn on thermochemical reactions and phase transitions and to suddenly create large-amplitude mechanical deformations and large defect densities.[1,2] In molecular liquids and solids, these phenomena can be probed by optical[3] or vibrational[4] spectroscopy, which allows molecular-level behavior to be investigated. Shock compression experiments are ordinarily carried out at large facilities such as government or military laboratories. Shocks are generated using explosive charges, gas-driven projectiles, or high-energy laser sources. The repetition rate is low, and the cost per shock is high. Among the more extreme examples are the use of nuclear explosives to investigate shock propagation in metals[5] or the giant Nova laser at Lawrence Livermore National Laboratory to investigate shock compression of deuterium.[6] However, even the more modest two-stage gas gun apparatus involves costs of perhaps $10^3 per shock. Although a gas gun can be fired on successive days, over the long term a typical repetition rate is perhaps once per week.

Shock compression of molecular materials involves extremely high-speed mechanical processes.[1,2] A typical shock velocity is a few km/s. At the molecular level, that works out to a few nm/ps, so shock waves in condensed matter propagate at a velocity of several molecular diameters per picosecond. There is evidence to suggest that the width of the thin nonequilibrium layer termed the "shock front" may in certain cases be just a few molecular diameters,[7−11] so clearly the dynamical process of shock compression can lie in the realm of ultrafast phenomena. Conventional shock methods are not well suited to investigate the ultrafast dynamics occurring behind the shock front, although there has been a bit of progress in this area.[10,11]

Ultrafast phenomena in condensed matter are ordinarily studied with high repetition rate picosecond or femtosecond lasers producing moderate pulse energies (≤1 mJ) and powerful signal-averaging techniques.[12] Most research in chemistry involves photochemistry or molecular energy transfer, phenomena which can be triggered by a UV, visible, or IR pulse. These phenomena are probed by a variety of techniques including absorption and fluorescence spectroscopies, and more recently sophisticated nonlinear and coherent spectroscopies such as four-wave mixing, photon, and vibrational echoes have become almost commonplace.[12]

If a simple way could be found to use common commercially available moderate-energy ultrashort pulse lasers to generate reproducible shock waves in condensed matter, then a revolution in shock wave technology could ensue. The ability to study shock phenomena would become much more widespread. Laboratories previously capable of studying only photoinduced phenomena could begin spectroscopic studies of matter under high-speed shock compression. All the powerful spectroscopic tools presently available to ultrafast spectroscopy laboratories could be brought to bear on shock processes in condensed matter. The level of sophistication of shock experiments, e.g.,

* To whom correspondence should be addressed. E-mail d-dlott@uiuc.edu; Fax 217-244-3186; Phone 217-333-3574.

S1089-5647(97)03404-4 CCC: $15.00
Published on Web 02/20/1998

studies of complex materials, layered materials, nanostructured materials, etc., would thereby increase as well.

The idea of using a benchtop picosecond pulse laser to generate and probe shock waves is hardly new. Several groups had performed experiments in the 1980s, using picosecond Nd:glass lasers to produce shock waves by intense optical pumping of thin metal foils.[13] However for several reasons interest and enthusiasm in these techniques had waned by the 1990s. Despite the use of picosecond pump and probe pulses, the time resolution of spectroscopic measurements was rarely better than 10 ns,[14] primarily limited by geometrical considerations discussed below, and the quality of the data turned out no better than in gas gun experiments.

Most conventional shock wave experiments are focused on determining thermodynamic properties, equations of state, and mechanical strength or failure mechanisms. It is usually thought such measurements are best made using long-duration (>several microseconds) planar shock waves propagating at constant velocity,[15] which produce step function shock compression. A great deal of the cost of shock generation by conventional methods is related to the energy costs of generating a longer duration shock. A 1 mJ laser pulse can make a quite powerful shock, but only if it is focused tightly (to perhaps $\sim$100 μm in diameter). However, a shock generated from a small diameter spot will not remain planar very long. A simple criterion for shock planarity is for the diameter to be more than 10 times the run distance.[15] A shock generated from a $\sim$100 μm diameter spot will run in a planar geometry for about 10 μm. That means the 1 mJ pulse can produce a steady shock with a duration of a few nanoseconds. Such a short duration need not necessarily be a disadvantage, if high-quality, high-speed optical and electronic measurement systems are used. A step function is not the only interesting way for making shock measurements. The δ-function, which is the sine qua non of pulsed laser spectroscopy, can also be a useful research tool. As we shall see below, many new and exciting research applications can be found for short duration "nanoshock" pulses.

To develop the nanoshock technique, several difficulties had to be overcome, especially geometrical factors relating to the time-of-flight mismatch between shock waves and light pulses. As discussed in the rest of this article, we have succeeded in developing a versatile technique involving a microfabricated shock target array system for generating and probing tiny but quite powerful shock waves at a high repetition rate, in *virtually any molecular material*. Although many in the shock wave community are pressing to use ever larger facilities (e.g., the proposed near-ignition facility, "NIF") to study the effects of ever more powerful shock waves on simple systems such as metals or hydrogen, our techniques open up the possibility for any research group equipped with ultrashort laser instrumentation to study in depth the effects of shock waves on complex systems of interest in chemistry, biology, and medicine.

In the remainder of this article, we provide a brief introduction to shock waves and our nanoshock methods. We then discuss studies of shock waves in anthracene. Anthracene is regarded as a model for molecular solids, and anthracene studies were used to develop and perfect the nanoshock technique. Some possible future research directions for shock waves are mentioned and illustrated briefly by examples from ongoing work involving energetic materials and biomaterials.

2. Shock Wave Basics

Figure 1 illustrates some basic features of shock waves.[16] Imagine a weight falling at velocity U_p onto a block of sample material of density ρ_0 (Figure 1a) at initial pressure P_0. In our experiments, it is not a falling weight but the rapid expansion of an exploding thin layer which launches the shock wave, but the basic concept is the same. If the velocity U_p is small, an acoustic wave front is launched (Figure 1b). The acoustic front moves through the sample at the speed of sound c_0, and the density ahead of and behind the front is ρ_0. If the velocity U_p is large (a significant percentage of the acoustic velocity c_0), then a shock front is launched (Figure 1c). When the falling weight hits the sample, the interface begins to move (flow) at approximately the velocity U_p, although the flow velocity is somewhat dependent on the relative shock impedances of weight and sample.[16,17] A shock begins to move through the sample at the shock velocity U_s. From elementary considerations of conservation of mass, momentum, and energy, the Hugoniot−Rankine relations can be derived,[1,16]

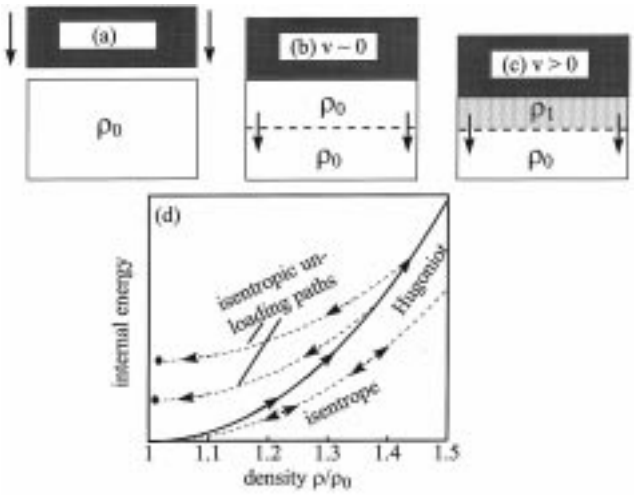

Figure 1. (a) A weight falls on a sample. (b) If the weight's velocity $U_p \sim 0$, an acoustic wave is launched, which moves at velocity c_0. (c) If the weight's velocity v is a significant fraction of c_0, a shock wave runs at velocity $U_s \approx c_0 + U_p$. The density behind the front ρ_1 is then greater than the ambient density ρ_0. (d) A reversible adiabatic compression follows the curve labeled "isentrope". After the compression unloads, the system reversibly returns to its initial state. A shock is an irreversible adiabatic compression which follows the curve labeled "Hugoniot". Subsequently, the system isentropically unloads to a final state with greater internal energy.

$$\rho_1 = \rho_0(1 - U_p/U_s)^{-1} \tag{1a}$$

$$P - P_0 = \rho_0 U_s U_p \tag{1b}$$

and

$$E - E_0 = {}^1/_2(P + P_0)(V_0 - V_1) \tag{1c}$$

where P is the shock pressure, ρ_1 is the density of shock-compressed material, and V_0 and V are relative volumes, $V_0 = 1/\rho_0$ and $V_1 = 1/\rho_1$. The shock velocity is roughly[1,16] the velocity of the flowing sample material U_p plus the acoustic velocity, $U_s \approx U_p + c_0$. For example, if the velocity U_p is 10% of the acoustic velocity ($0.1c_0$) and the shock moves at $U_s = 1.1c_0$, then eq 1a shows that $\rho_1 = \sim 1.1\rho_0$.

Shock compression is a fast irreversible process which is always adiabatic.[1] Consider the adiabatic *reversible* (isentropic) compression of a solid from initial density ρ_0 to final density ρ_1. Isentropic compression occurs when the rate of pressure change is small enough that the pressure inside the solid tracks the external driving pressure. As shown in Figure 1d, the

internal energy during compression increases along the curve denoted "isentrope". Of course, the temperature and pressure increase as well.[1] When the compression is released, the solid quickly expands back to its initial state. Although this pressure release process occurs quickly, it is inherently a reversible expansion[1] (vide infra) along the isentrope.

When a solid is shock compressed, the energy increase follows an *irreversible adiabat*[1,16] termed the "shock adiabat" or "Hugoniot". Hugoniot is the term used for a family of relations between the shock velocity, pressure, and density. Usually Hugoniot data are given in the form

$$U_s = b + mU_p \tag{2}$$

Tables of the parameters b and m in eq 2 can be found in the literature (especially ref 16) for various materials. Equation 2 can be combined with eqs 1 to yield a series of useful relations such as

$$U_s = b/(1 - m\Delta V) \tag{3}$$

or

$$p = b^2\Delta V/[V_0(m\Delta V - 1)^2] \tag{4}$$

where $\Delta V = 1 - V_1/V_0$.

The internal energy and temperature are always greater along the Hugoniot than along the isentrope. When shock compression is released (shock unloading), the solid expands reversibly along an isentrope such as one of the isentropic release paths in Figure 1d. After a cycle of shock compression and unloading, there is a net increase in entropy ΔS_{irr} and in temperature ΔT_{irr}. In other words, after the cycle there is residual heat in the sample.

The compression shock front is a sudden jump in density. In continuum fluid mechanics, the front is found to be a discontinuity where pressure, temperature, density, and entropy increase instantaneously.[1] To see that, think of a slowly rising shock front as consisting of a leading, lower pressure shock followed by a trailing higher pressure shock. Since the higher pressure shock travels faster, the shock front will steepen up until it becomes discontinuous. In contrast, the expansion shock front is not sharp. If the expansion front were a sharp discontinuity, there would be a sudden entropy decrease across the front, in violation of the second law of thermodynamics.[1] Therefore, the expansion process must be reversible.

In real materials the shock front is not a sudden discontinuity, but instead consists of a thin nonequilibrium region whose detailed structure depends on the material.[17−21] It is well-known in shocked *molecular* gases that that translational temperature behind the front rises over a distance about equal to one mean free path, but the vibrational and rotational temperatures rise over a greater distance.[1] Almost nothing is known about the detailed structure of the front in shocked *molecular* liquids and solids. Behind a solid-state shock front, the phonon temperature rises over a distance thought to be quite short (perhaps a few nanometers),[21] and the vibrational temperature rises over a longer distance (perhaps 100 nm).[22,23] Additional and even more complicated shock front structures can exist, when chemical reactions and mechanical processes such as plastic deformation and defect generation are considered.[19,20] One interesting problem that has not yet received much consideration is the quite complicated mechanical response to a shock front, of a molecular material with a complicated nano- and microstructure, such as a protein, a membrane, a silk thread, etc.

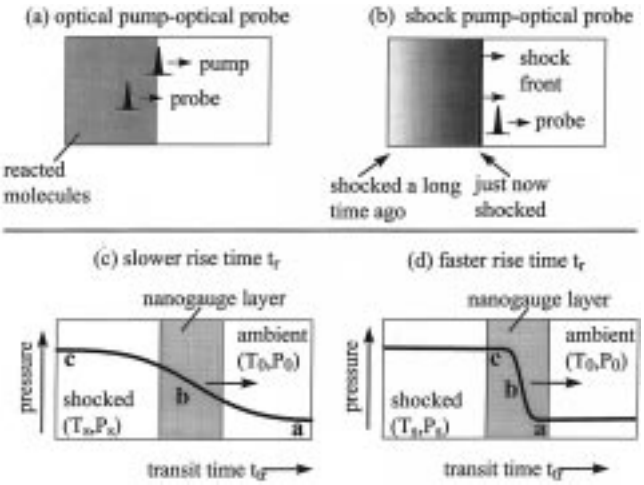

Figure 2. (a) An optical pump, optical probe experiment. The two pulses propagate through the sample at roughly the same velocity. (b) A shock front pump, optical probe experiment. The probe pulse moves so much faster than the shock front that it probes molecules right behind the front as well as molecules shocked a long time ago. Picosecond time resolution can be obtained only if the sample thickness is of nanometer order. (c, d) A shock front running through a thin nanogauge layer (shaded region) in an impedance-matched sandwich. The shock raises temperature and pressure from ambient (T_0,P_0) to (T_s,P_s). (c) In the slower rise time limit, the layer is reversibly compressed because the pressure rises slowly and uniformly throughout the nanogauge layer. (d) In the faster rise time limit, the shock front cuts the nanogauge into three parts. Parts a and c consist of ambient and shocked material, respectively. In region b, material exists in a range of pressures between P_0 and P_s.

3. Probing Shock Fronts

The problem with probing shock fronts is that shock waves moving at a velocity of a few nm/ps are very slow compared to light moving a few hundred μm/ps. If we wish to probe only those molecules right behind the shock front (say within a few picoseconds of the shock front), then ideally a quite high spatial resolution of a few tens of nanometers is needed.[14] That spatial resolution cannot be attained merely by focusing laser pulses tightly because it is much smaller than a wavelength of visible light. Instead, we use a sample with a nanometer scale thickness layer. The problem with a very thin layer is getting ultrafast spectra with good signal-to-noise.

Figure 2a,b illustrates the problem another way. Figure 2a shows how high time resolution is obtained in conventional photochemistry experiments, where time resolution as good as a few tens of femtoseconds has been obtained.[12] The pump pulse creates a traveling photochemistry "front" moving at the speed of light in the sample. At any particular delay time, the probe pulse(s) trail behind the pump pulse a fixed distance, while both propagate through the sample. A rather long interaction length (sample thickness) can be used, limited only by the spreading and velocity mismatch of the pump and probe pulses due to dispersion.

Figure 2b shows a shock probed by an optical pulse. In Figure 2b, the shock front is about halfway through a thick sample. When the probe pulse runs through the sample at the speed of light, it sees material right behind the shock front, and in addition it sees all the material that was shocked a long time previously. The result is a spectrum with degraded time resolution. The time resolution in this geometry decreases as

the sample thickness increases, and it is on the order of the shock transit time through the sample. For a sample whose thickness is even just 10 μm, the time resolution will be at best a few nanoseconds.

To obtain high time resolution of shock front effects, the probe pulse must interrogate only a very thin region. Some researchers have used ultrashort pulses or high-speed streak cameras to look at shock front breakout at a free-surface interface.[10,24] This method provides high spatial resolution only for opaque materials, not for transparent dielectrics because the probe pulses see into the sample a distance roughly equal to the absorption length. For metals[24] this length is a few nanometers. For silicon in the visible, it is about 10 nm.[10] The free surface method introduces a complication because it monitors the shock front as it reaches an interface with a sudden discontinuity in shock impedance.[17] This situation is more difficult to analyze than a shock front which is steadily propagating through a region of constant shock impedance.[18]

In our experiments, we monitor the effects of the shock front using a sandwich arrangement containing a nanolayer termed an "optical nanogauge",[25−29] as shown in Figure 2c,d. The nanogauge and polymer layers are approximately matched[14,26] in shock impedance (the shock impedance is the acoustic velocity times the density[16,18]), so there is little or no reflection of the shock front at the various interfaces. The shock front transit time across the nanogauge is denoted t_{tr}. For the typical nanogauges used so far, of thickness 300−700 nm, $t_{tr} \approx 60-180$ ps. The response time of the nanogauge is on the order of t_{tr}. The shock front rise time is denoted t_r. Figure 2c,d illustrates two important cases of interest,[28,29] where the rise time $t_r \gg t_{tr}$ and where the rise time $t_r \ll t_{tr}$.

When the shock front passes through the nanogauge layer, the temperature and pressure rise from the ambient values of (T_0,P_0) to the "shocked" values (T_s,P_s). Many spectroscopic techniques have been used to probe shocked molecular materials[3,4,11,30] including emission, absorption, and Raman scattering. All such spectra are sensitive to T and P in one way or another, as described in texts on molecular spectroscopy.

In Figure 2c, the shock front has a rise time t_r which is *slower* than the shock transit time t_{tr}. In this case, the pressure everywhere inside the nanogauge is about equal to the pressure at the surface of the nanogauge, so the compression process is nearly isentropic.[26,29] As the shock pressure slowly rises, the spectrum of the nanogauge layer will gradually evolve,[26] on the time scale of t_r, from the spectrum of material at (T_0,P_0) into the spectrum of material at (T_s,P_s).

In Figure 2d, the shock front has a *fast* rise time, $t_r \ll t_{tr}$. There is a sudden jump in pressure in the nanogauge, and shock compression is irreversible.[26,29] In this fast rise time case, the nanogauge spectra are qualitatively different[28,29] from the slow rise time case above. For a step-function rise of the shock front ($t_r = 0$), the spectrum at any time is a superposition of the spectrum of (T_0,P_0) uncompressed nanogauge material and (T_s,P_s) compressed nanogauge material. If the shock front has a finite rise time, $0 < t_r \ll t_{tr}$, the spectrum is a superposition of the (T_0,P_0) and (T_s,P_s) spectra (regions a and c in Figure 2d), plus an additional contribution[27,28] from material at intermediate pressures, $P_0 < P < P_s$. In this case it is possible to determine the rise time t_r even when the transit time t_{tr} is quite a bit more (say perhaps 10 times more) than the rise time t_r. The rise time t_r can be deduced by determining what fraction of the spectral intensity[28,29] comes from region b, relative to that from regions a and c in Figure 2d. The ability to resolve very short rise times improves as the transit time t_{tr} becomes smaller, but in a different way than in the slow rise time case above.[29] The fraction of shocked material from region b, relative to regions a or c, is roughly t_r/t_{tr}, so it becomes more difficult to discern the spectral contribution from region b when $t_{tr} \gg t_r$.

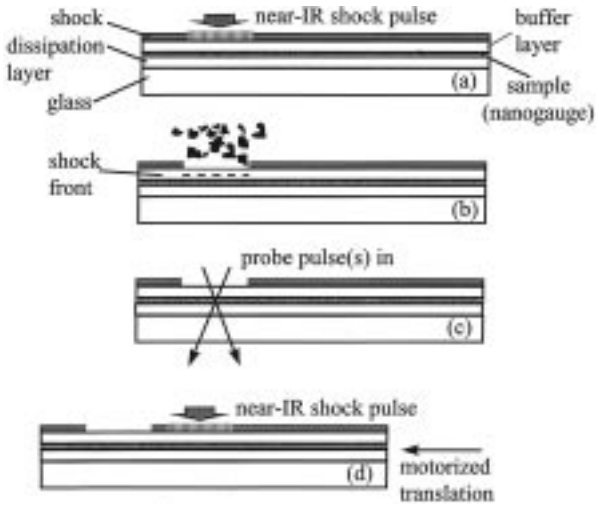

Figure 3. Schematic of a microfabricated shock target array with a nanometer thickness sample layer (optical nanogauge) sandwiched between a micrometer thickness buffer layer and dissipation layer. Near-IR ablation of the shock layer launches a nanoshock through the sample layer. The shock front reaches the nanogauge, and its effects are probed, some time after the shock generation layer has ablated away. Adapted from ref 26.

4. Experimental Methods

The conceptual design of shock experiments with the multilayered microfabricated shock target array is shown in Figure 3. There are many possibilities for array design and construction, which depend on the desired shock rise time and shock duration, and the properties of the sample material. The shock is generated by ablation of a thin outer layer, the shock generation layer, consisting of an absorbing dye and an energetic binder.[26,27] The rise time and duration of the nanoshock depend on the pump pulse duration (~150 ps in our experiments), the thickness of the shock generation layer, the absorber concentration, and the thickness of the buffer layer.[26]

The buffer layer has two functions. First, it delays the shock arrival by a few nanoseconds, giving enough time for the shock generation layer to ablate away before the probe pulses arrive.[26] Second, if the thickness of the buffer layer is properly chosen, it allows the shock front to steepen up before it reaches the sample.[26,31,32] In fact, the shock front at the sample layer can become quite a bit steeper than the shock generation pulse duration of ~150 ps. After passing through the buffer layer, the shock propagates through the sample layer and into a dissipation layer where it dissipates by spherical expansion, when the rarefaction waves generated at the edges of the shock reach the center of the shock.

In construction of an array, it is important that a layer not be dissolved by the solvents used to apply subsequent layers. Taking as a specific illustration our anthracene experiments,[29] the dissipation layer is applied first to the glass substrate. It is a 7 μm thick layer of polybutadiene, applied by spin coating from hexane solution. Anthracene is applied next, by spraying a solution of anthracene in acetone (which does not dissolve polybutadiene), through a nozzle which produces a fine mist. The anthracene layer consists of a dense mass of nanocrystals, whose density is within 5% of the density of crystalline

anthracene.[25] The buffer layer, consisting of poly(vinyl alcohol), is applied next by spin coating an aqueous solution of poly-(vinyl alcohol), which does not dissolve anthracene or polybutadiene. Finally, the shock generation layer, consisting of IR-165 dye (with an absorption maximum near the 1.064 μm wavelength of the Nd:YAG laser) and a PMMA (poly(methyl methacrylate)) binder,[26,29] is spin coated from a solution of ketones which do not dissolve the underlying layers. PMMA undergoes highly exothermic thermal decomposition. An option is to spike the shock generation layer with a bit of high explosive booster such as RDX, to attain higher shock pressures.[29]

5. Experiments on Anthracene

Anthracene was chosen for these experiments because it is regarded as a model system for molecular crystal studies.[33] The isothermal compressibility,[34] the Hugoniot,[35] and many other physical properties[33] of anthracene are tabulated in reference sources. In crystalline anthracene, the totally symmetric vibrations have large Raman cross sections and narrow line widths,[36,37] which makes it easy to detect frequency shifts or line broadening effects due to shock.

The anthracene experiments used broad-band multiplex picosecond CARS spectroscopy,[38,39] which here generates an entire CARS spectrum over an ~150 cm^{-1} range on each shot.[39] The spectra displayed below are the average of ~5000 laser shots, which provides a high signal-to-noise ratio despite the thin (~500 nm) nanogauge layer. We studied the most intense Raman-active anthracene vibrational transition,[35] denoted ν_4, at a nominal Raman shift of 1404 cm^{-1}.

In all molecular materials, the Raman frequency shifts and widths change with temperature and density. Density can be converted to shock pressure[27] when the Hugoniot is known. The specifics of density and temperature effects depend on details of the anharmonic intermolecular potential,[39] which are difficult to calculate from first principles.[41] We ordinarily determine these effects empirically using calibration Raman spectra from a thermostated diamond anvil cell apparatus.[26] To determine the shock temperature and pressure T_s and P_s from a CARS spectrum, one needs at a minimum two observables. One possibility is simultaneously monitoring the shift of two or more Raman transitions[42] (e.g., see the NTO data in Figure 11). Another is monitoring the width and shift of a single transition.[26−29]

In anthracene, we have calibrated the ν_4 transition.[26,27] It was found[26] that isothermal compression, which increases density alone, caused ν_4 to blue shift but not broaden. Constant pressure heating corrected for thermal expansion,[27] which is tantamount to increasing temperature alone, caused ν_4 to broaden but not shift. Thus, by looking at the frequency shift and width, it is possible to estimate the temperature and density (and thereby the shock pressure[27]) from the vibrational spectrum. We believe the accuracy of this method to be[27] about 5% and that its accuracy can be improved by looking at several calibrated transitions simultaneously. Figure 4 shows a vibrational spectrum of anthracene at ambient temperature and under shock load. The peak blue shift is ~16 cm^{-1}, and the width increases from 4 to 6 cm^{-1}. According to our calibration data, that corresponds to $P_s \sim 4.2$ GPa and $T_s \sim 350$ °C.

In all the shock data displayed below, time $t = 0$ always refers to the arrival of the near-IR pulse at the shock target array, which is known accurately from optical correlation measurements.[26] The arrival time of the shock front at the sample layer is not a constant. It depends on how the target array is constructed and how fast the shock propagates.[26] The arrival time is typically in the 1.5−3 ns range in our experiments. In Figure 5 we show spectra of a 500 nm thick nanogauge with a shock transit time of $t_{tr} \sim 125$ ps. The shock front reaches the nanogauge at $t \sim 3$ ns. A single peak in the Raman spectrum is observed, which first blue shifts (pressure increasing) and then red shifts (pressure decreasing). As described in the discussion associated with Figure 2c, these spectra indicate the shock front rise time t_r is slower than the ~125 ps transit time, which is approximately equal to the nanogauge response time. Therefore, the nanogauge undergoes a nearly isentropic cycle of compression and unloading. A plot of the time-dependent peak frequency shift[26] in Figure 5 gives the shock front rise time as ~400 ps, the fall time as ~2 ns, and the peak pressure as $P_s = 3.0$ GPa. (This pressure was incorrectly given as 2.6 GPa in ref 27.)

In Figure 6 we show data from a ~700 nm thick anthracene nanogauge using a shock generation layer that produces a very fast shock rise time. After the shock front reaches the nanogauge at t ~1.45 ns, the intensity of the ambient pressure peak decreases, and a second peak due to compressed anthracene grows in. This is a remarkable series of shock spectra. From Figure 6 *alone* we can obtain the shock temperature and pressure, the shock front rise time, and the shock velocity.[29]

The spectra in Figure 6 have been analyzed by singular value decomposition (SVD), a well-known mathematical method.[43,44]

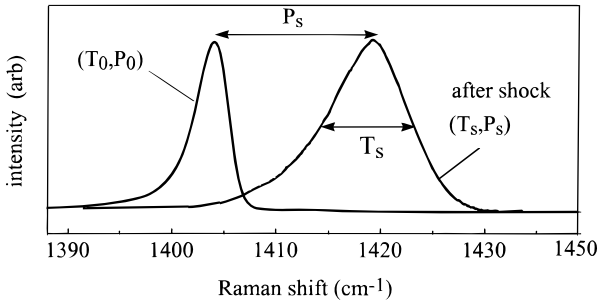

Figure 4. Coherent Raman (CARS) spectra of anthracene ν_4 vibrational transition of a 500 nm thick polycrystalline layer under ambient conditions at (T_0,P_0) and under shock loading at (T_s,P_s). The peak shift increases with increasing density but is nearly independent of temperature. The peak width increases with increasing temperature but is nearly independent of density. The shift can be used to estimate pressure and the width can be used to estimate temperature. Here $P \approx 4.2$ GPa and $T \approx 350$ °C. From ref 45.

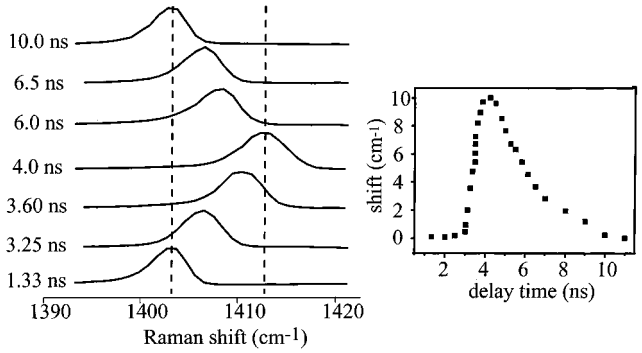

Figure 5. CARS spectra of anthracene ν_4 as a 3.0 GPa shock passes through a 500 nm thick layer. The single peak which blue shifts and then returns to its initial shift indicates a cycle of reversible compression and expansion, because the shock front has a rise time slower than the transit time across the layer, as in Figure 2c. The time dependence of the peak frequency shift is shown at right. The shock arrives at ~3.2 ns (relative to the arrival of the near-IR shock generation pulse at $t = 0$). The rise time is 400 ps and the fall time is 2 ns. Adapted from ref 26.

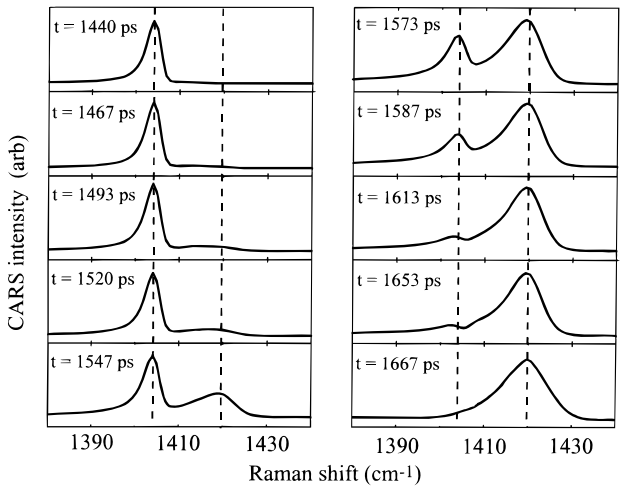

Figure 6. CARS spectra of 700 nm layer of anthracene with a 4.2 GPa shock. The two-peak structure indicates the shock front has a rise time far less than the 175 ps transit time, as in Figure 2d. The shock arrives at 1.45 ns (relative to the arrival of the near-IR shock generation pulse at $t = 0$). Mathematical analysis of the data shows the shock front rise time $t_r < 25$ ps. From ref 28.

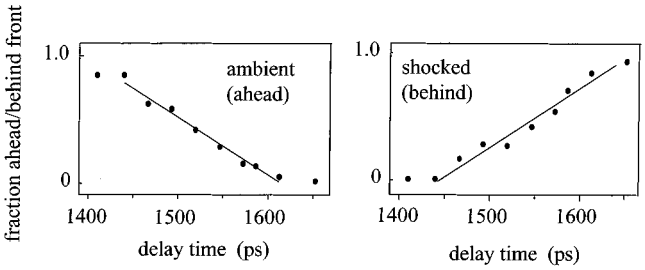

Figure 7. Time-dependent fraction of material ahead of and behind the shock front, obtained from analysis of the spectra in Figure 6. The fraction ahead and behind the front is proportional to the square root of the intensity of the lower and higher frequency peaks, respectively. These results determine the time the shock front enters and leaves the anthracene layer and show the shock front velocity remains constant while the front is in the layer. Knowing the layer thickness is 700 nm, the shock front velocity is found to be 4.0 km/s. From ref 29.

SVD analysis shows that *every spectrum* in Figure 6 can be generated using only a set of time-dependent coefficients and exactly two basis spectra,[28] which are identical within experimental error to the first and last spectra in Figure 6. In other words, every spectrum is solely a superposition of the spectra of ambient and shocked material, and there is absolutely no observed contribution[28] from material at any pressure other than P_0 and P_s. That shows the shock front rise time t_r must be very short indeed. Error limits set by this analysis[28] give the rise time $t_r < 25$ ps and the width of the front (region b in Figure 2d) as <100 nm. Since an anthracene molecule is about 1 nm, that means the front is less than ~100 molecules wide.[28]

The coefficients of the basis spectra obtained by SVD analysis represent the time dependence of the relative intensities of the ambient (T_0,P_0) and shocked (T_s,P_s) contributions to the spectra in Figure 6. The fraction of the nanogauge ahead of and behind the front is proportional to the square root of these coefficients,[29] since the CARS signal is proportional to the *square* of the amount of material.[38] In Figure 7 we plot these fractions versus time. Then by knowing the thickness of the nanogauge, the shock velocity can be found. The velocity is constant as the front moves through the nanogauge, and it is[29] 4.0 km/s, compared to the ambient speed of sound in anthracene[33,35] of ~3.2 km/s.

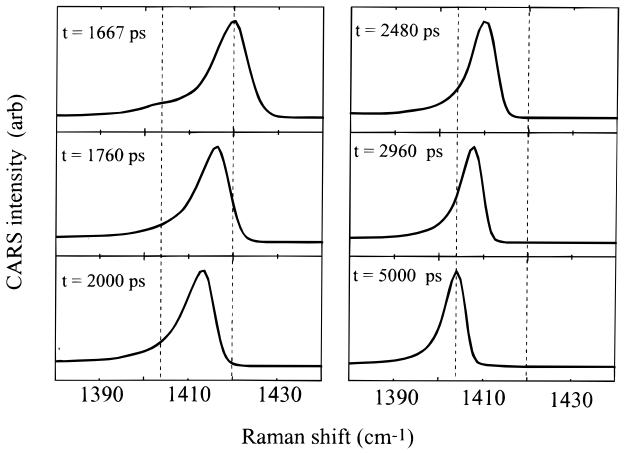

Figure 8. Anthracene spectra during reversible unloading of a 4.2 GPa shock. The spectrum at 1667 ps is the same as the last panel of Figure 6. As the shock unloads, the spectral width narrows and the peak returns to near its initial shift. The ultrafast peak narrowing indicates ultrafast cooling due to adiabatic solid-state expansion. The cooling rate is a few hundred billion degrees per second.

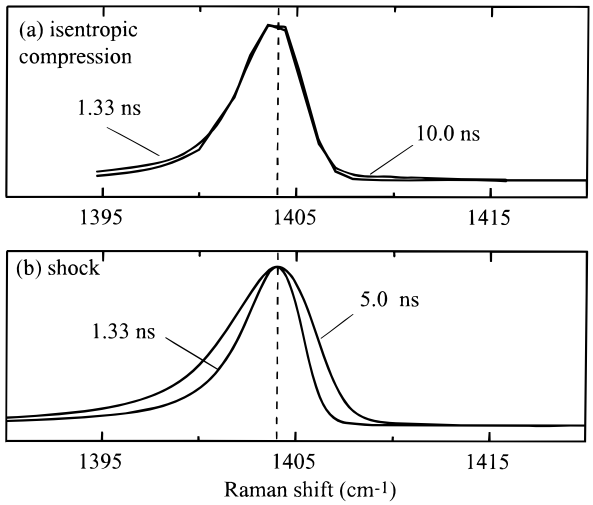

Figure 9. CARS spectra of anthracene before and after a nanosecond cycle of shock compression and unloading. (a) Before (1.33 ns) and after (10.0 ns) an isentropic cycle with peak pressure 3.0 GPa. (b) Before (1.33 ns) and after (5.0 ns) a cycle of irreversible shock compression and reversible unloading with peak pressure 4.2 GPa. The increase in line width after this latter cycle is attributed to residual heat due to entropy increase across the shock front. From refs 26 and 29.

Shock unloading in anthracene is seen in Figure 8. As the shock unloads the spectral peak shifts back to near its original location, and the spectrum narrows. The narrowing is indicative of rapid cooling due to adiabatic expansion, from a high temperature of ~350 °C back to about 80 °C. The cooling rate is extremely large, *a few hundred billion degrees per second*.

Figure 9 compares anthracene Raman line shapes before and after a *cycle* of rapid compression and expansion. With the nearly isentropic compression of Figure 5, the line shapes before and after the cycle are identical. With irreversible compression by the very fast shock front, the line shape after this cycle is somewhat broader. The broadening indicates a temperature of about 80 °C and is a consequence of residual heating caused by the entropy increase across the shock front.[27]

6. Nanoshock Pulses

Typical nanoshock waveforms[26,29] generated in anthracene are represented in Figure 10. One type of pulse has a rise time

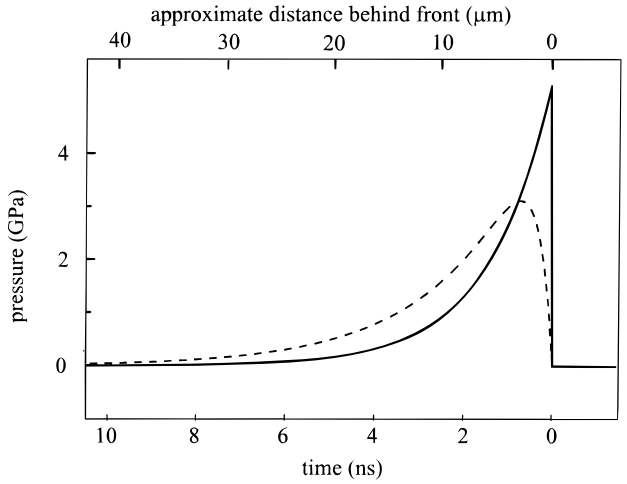

Figure 10. Nanoshock pulse waveforms reconstructed from CARS data in Figures 5, 6, and 8. The solid curve represents a nanoshock with a fast rise time (t_r < 25 ps) which produces irreversible compression and reversible expansion. The broken curve represents a nanoshock with a slower rise time (t_r = 400 ps), which produces isentropic compression and expansion. The amplitudes of the nanoshock pulses can be varied in the 0−5 GPa range.

t_r less than 25 ps, which generates a strongly irreversible compression. The fall time is 1.5 ns and the peak pressure 4.2 GPa. The other pulse has a slower rise time of 400 ps, which generates a nearly reversible compression. The fall time is 2 ns and the peak pressure 3.0 GPa. By varying the properties of the shock generation layer, we can make the rise time as long as[26] 800 ps, and we can continuously vary the peak pressure from zero to a maximum of about 5 GPa using the present laser system, which provides a maximum shock pulse energy of 0.15 mJ.

In considering research applications for nanoshocks, there are three ways to think about the nanoshock technique:[45]

1. A *Sudden Ultrafast Uniaxial Compression.* The rise time of the shock compression pulse can be shorter than the time scales for most mechanical relaxation processes. The passage of the steeply rising nanoshock front (a step function) will create a dense sea of highly nonequilibrium mechanical excitations.[22,28] These will consist of intermolecular excitations (phonons) which push molecules around and can cause phase transformations, plastic deformation, defect formation, etc., and intramolecular excitations (molecular vibrations).

2. A Sudden Jump to High Temperature and Pressure (T_s,P_s). After nonequilibrium transients related to the sudden uniaxial compression have had time to relax, at the peak of the nanoshock pulse is a brief (few hundred picoseconds duration) period of nearly stable shock loading. During this period of quasistatic loading, steady spectroscopic measurements can be made of nonreactive materials under extreme conditions, or the kinetics of thermochemical reactions can be probed at high temperature and pressure.

3. A Fast (Nanosecond) Cycle of Compression and Decompression. A molecular material is rapidly compressed and heated, then decompressed, and rapidly quenched (cooled) by a δ-function shock pulse. The properties of these rapidly quenched metastable states can be studied, and mechanical relaxation processes occurring on the nanosecond or longer time scales can be studied spectroscopically.[45,46]

7. Applications of Nanoshocks in Research

Nanoshock pulses can be viewed as an alternative way of doing time-resolved spectroscopy, in contrast to the more conventional methods of direct optical pumping of the sample. In the nanoshock method, the interactions between the shock generation layer and the intense pump pulses are difficult to understand in detail. However, these complexities resolve themselves into a rather simple situation of fast uniaxial compression, by the time the shock passes through the buffer layer and reaches the sample. Thus, with nanoshock pulses it is possible to put a tremendous amount of energy into the sample, without dealing with the complexities of condensed matter irradiated by very high-power optical pulses. In this section we briefly discuss some of the interesting research possibilities for this technique. In the next section we illustrate some of these possibilities with brief examples from ongoing research in our laboratory.

1. Optical Studies of Materials under Extreme Conditions. With a conventional static high-pressure and high-temperature apparatus, it takes some time (typically microseconds or longer) to get the sample up to temperature. During that time the sample might decompose or be damaged. With nanoshocks, the pressurizing and heating process occurs on the subnanosecond time scale. It thus becomes possible to obtain spectra of materials that react or decompose too quickly to study by conventional means, for example, large organic and biomolecular systems which have never been studied at high temperatures and pressures. With a nanoshock, it is likely possible to drive a sample past a phase boundary faster than the phase transition can occur, allowing the dynamics of phase transformations to be investigated.

2. Ultrafast Thermochemistry. The nanoshock produces a very fast temperature jump (*T*-jump) which can suddenly initiate a thermochemical reaction. The amplitude of the fast temperature jump from shock compression can be much greater than an equally fast laser *T*-jump, since the latter is limited to pulses that are weak enough to avoid shock wave generation or dielectric breakdown. An interesting feature of the nanoshock pulse is the rapid *turn-off* time, which is much faster than an ordinary *T*-jump experiment, where cooling occurs by the far slower process of thermal diffusion.[47] In photochemical studies, it is straightforward to control a chemical reaction by turning it on and off with a light pulse. Now by using a nanoshock, a thermochemical reaction can be rapidly (a few nanoseconds) turned on and then turned off. During a thermochemical reaction at high temperature, it is hard to monitor reactive chemical intermediates because they are consumed quickly, and spectral transitions are broadened by the high temperature. With a nanoshock, the reaction can be suddenly turned off, and these intermediates can be frozen and studied at low temperature.

3. Highly Vibrationally Excited Molecules. When a nanoshock front passes through a material, a great deal of mechanical energy is added on average to *every molecule behind the nanoshock front.* In the anthracene experiment, the shock energy increase is ∼10 000 cm^{-1} of thermal energy and ∼50 000 cm^{-1} of potential energy per molecule. The coupling between the shock front and each mechanical degree of freedom is specific,[22] so a specific (nonthermal) excitation can be produced when the shock front rise time is faster than the time scales for vibrational energy redistribution. For example, the shock front couples more efficiently to intermolecular excitations (phonons) than to intramolecular excitations (molecular vibrations),[21,22] so an initial large excess of phonons is generated behind the front. In polyatomic molecular materials, vibrational energy redistribution processes typically occur on the 10−100 ps time scale,[14,23,48,49] so the faster rise time (<25 ps) nanoshock fronts

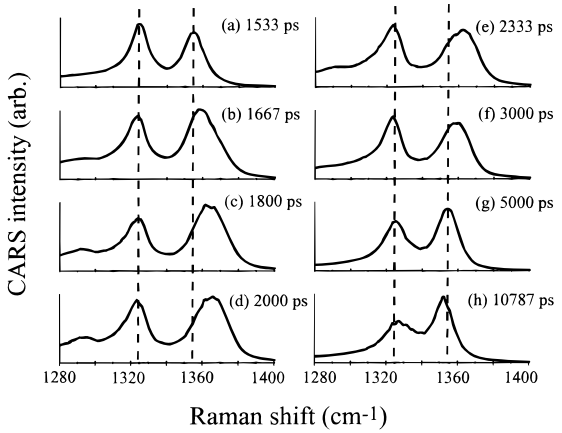

Figure 11. Time-dependent CARS spectra of a thin (~1 μm) layer of NTO high explosive with a 4 GPa shock which arrives at 1.7 ns. During the period of maximum shock loading (c−e) a third peak temporarily appears at lower frequency (~1295 cm^{-1}). After the shock is over (g, h), the lower frequency peak undergoes a nanosecond time scale decrease in peak intensity, which is due to an increase in the peak width (fwhm). From ref 45.

are clearly capable of producing highly nonequilibrium vibrational excitations in molecular materials.[28]

4. Large-Amplitude Molecular Dynamics. Important basic processes such as phase transformations, chemical reactions, enzyme and nucleic acid function, etc., involve relatively quite large, typically angstrom-scale, displacements. Therefore, it is very interesting to probe molecular dynamics induced by large-amplitude perturbations. Our nanoshock pulses produce typical compression factors[27] of 10−20%. For example, in a protein or membrane measuring 50 Å across, the driven dynamic molecular displacement may be 5−10 Å.

8. Ultrafast Material Relaxation in Molecular Crystals

In recent experiments on molecular crystals,[45,46] we have found a system that demonstrates the feasibility of studying mechanical relaxation processes which are produced by nanoshock and which have a characteristic time dependence which continues after the shock is over. The material studied was polycrystalline NTO (5-nitro-2,4-dihydro-3*H*-1,2,4-triazol-3-one), a new high-performance insensitive energetic material.[50] Picosecond CARS spectroscopy was used to monitor the region near 1350 cm^{-1}, where NO_2 stretching and N−H bending vibrational transitions are observed.[51]

Shock (~4 GPa) CARS spectra of NTO are shown in Figure 11. There are three interesting features in Figure 11 to note: (1) two prominent peaks in the vibrational spectrum which show different shifting and broadening responses to shock; (2) a small peak which temporarily appears near 1290 cm^{-1} only during the period of peak shock loading; (3) well after the shock has unloaded (t > 5 ns) the height of the lower energy peak continues to decrease on the nanosecond time scale. The third observation is evidence of a material relaxation process which continues after the nanoshock pulse is over.

In Figure 12a, we plot the time-dependent peak shift and peak width (fwhm) of the two vibrational transitions seen in Figure 11. The higher frequency peak has a much larger shock frequency shift than the lower frequency peak. Following the time dependence of the shift, we see the shock arrive at ~1.7 ns. The shock is over at ~5 ns. The irreversible nature of shock compression is evident, since the peak shifts do not quite return to their ambient values at longer times.

To study the time dependence of the peak heights, the CARS line shapes were analyzed with a routine that fits each spectrum

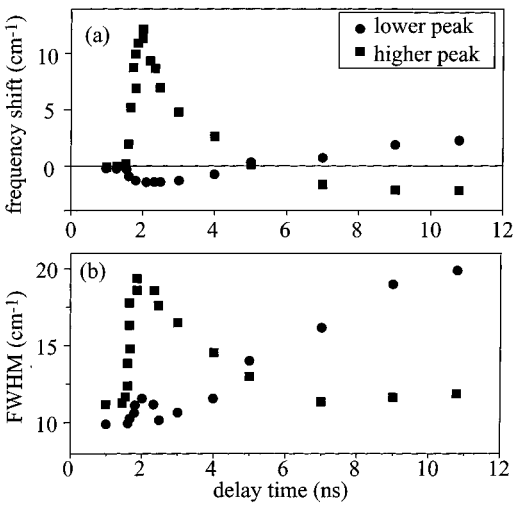

Figure 12. Time dependence of (a) peak shift and (b) peak width (fwhm) of two Raman transitions of NTO (see Figure 11) with a 4 GPa nanoshock. The peak shift data indicate the shock is over at ~5 ns. The time-dependent increase in fwhm of the lower energy peak indicates a nanosecond time scale material relaxation process which continues after the shock is over.

in Figure 11 to a superposition of Voigt line shapes. At any time, the ratio of the integrated intensities of the two main peaks remained constant. However, the width (fwhm) of the lower frequency peak increased with time, which accounts for the decrease of its height on the nanosecond time scale. The time dependence of the fwhm of the two main peaks is shown in Figure 12b. The higher energy peak behaves normally. It broadens temporarily during the period of maximum shock loading and then returns to a steady width after the shock which is slightly greater than the ambient fwhm. The lower energy peak shows unexpected behavior. Its fwhm increases a bit during the shock and then recovers. Subsequently, the fwhm almost doubles as the width continues to increase even beyond 5 ns, well after the shock is over.

More work is needed to fully understand the nanosecond time scale broadening process, but here are two plausible possibilities: (1) when the shock unloads, the NTO, which is initially present in the α-phase, undergoes a transition to the β-phase, which has a lower density (1.878 g/cm^3) than the α-phase (1.92 g/cm^3);[50] (2) when the shock unloads, the NTO crystals experience a large tensile load, which causes a high density of defects to be generated. The defects are observed as a time-dependent increase in the spectral width, which is presumably an increase in the inhomogeneous line width.

9. Shock Dynamics in Biomaterials

A novel application for shock waves being pursued in our laboratory involves shock wave dynamics of biological materials. Biomolecules and biomaterials have a complex structure and an equally complex mechanical response. Nanoshock techniques permit the study of these mechanical responses under conditions of large-amplitude displacements. The large-amplitude regime of the potential surface is particularly significant, since the functional motions of biomolecules almost always involve large-amplitude motions.

Biomaterials have not been much studied by conventional shock wave techniques. Our first experiment in this area[45,46] is an investigation of the heme protein myoglobin (Mb). Mb is a molecular nanomachine (see Figure 13a) about 4 nm in diameter, whose function is oxygen storage and release.[52] Mb is a mainly helical protein (eight helices) which binds a

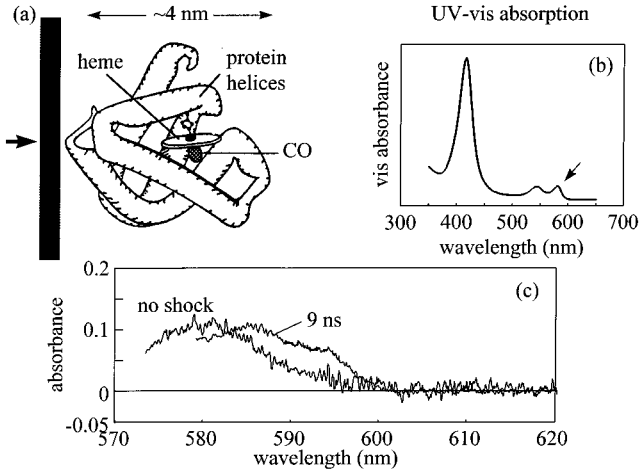

Figure 13. (a) Artist's conception of a shock front hitting a myoglobin−CO (Mb−CO) molecule. (b) UV−visible absorption spectrum of a microfabricated shock target array containing a 5 μm thick layer of Mb−CO in glycerol:water. The arrow indicates the spectral transition being probed. (c) Transient absorbance spectra of Mb−CO layer with no shock and a few nanoseconds after the shock is over (9 ns delay time). The heme spectrum is dramatically perturbed by the shock, and it does not relax back to its initial state on the <10 ns time scale.

prosthetic group, protoheme.[53] Oxygen, carbon monoxide, and other ligands bind at an active site of the heme.[53]

The phase diagram for native and denatured forms of Mb has been known for more than 20 years.[54] In equilibrium at 1 atm pressure, Mb becomes denatured when the temperature is raised to $T = 80$ °C. At room temperature, Mb becomes denatured when the pressure is raised to 0.6 GPa. Therefore, our nanoshock pulses can produce temperatures and pressures far greater than those required to denature the protein, but for a very short (nanoseconds duration) time period. These extreme conditions are expected to cause a very large structural distortion of Mb, but exactly what will happen we cannot yet say, due to a lack of knowledge of the *dynamics* of denaturation and unfolding. Certainly the tertiary structure will be greatly perturbed by the nanoshock pulse. When aqueous solutions are shocked, there can be a dramatic change in pH and ionic strength, and under some circumstances hydrogen bonding can become unstable,[55] so it might even be possible to greatly perturb the protein secondary structure with a nanoshock.

Following the brief period of high temperature and pressure caused by the nanoshock pulse, the protein sample is cooled so fast by adiabatic expansion that Mb should be frozen into metastable configurational states. The quite interesting structural relaxation processes, which result as proteins return to their equilibrium configurations, can be monitored by optical spectroscopy of the heme, which has an intense absorption in the visible or near-IR.[56] Other probe methods such as resonance Raman spectroscopy of heme[57] or fluorescence lifetime spectroscopy of tryptophan[58] are possible as well.

In our first experiments[45,46] with Dr. Jeffrey Hill, now at Coe College, we have demonstrated it is possible to fabricate a biocompatible shock target array, where the Mb protein (bound to CO for increased stability) is present in its native folded configuration. The sample is a thin layer of Mb−CO solution in aqueous buffer, with glycerol added to stabilize the layer. The absorption spectrum of heme in the Mb−CO shock target array is shown in Figure 13b. Using this array, we have made some preliminary studies of shock effects on Mb. We observed a dramatic change in heme absorption at the peak of shock compression. At delay times up to 10 ns, after the shock has unloaded completely, the Mb spectrum did not return to its initial state. Either the protein has been permanently damaged, or it will eventually relax back to its native state. This work will be continued by monitoring the heme over longer time scales and by varying the amplitudes of the nanoshock pulses. These early experimental results illustrate the potential application of the nanoshock technique to biological materials, unconventional materials, or precious materials available only in tiny quantities. Future applications of nanoshocks in biomaterials might involve the study of membranes, cells, and tissues.

10. Concluding Remarks

Using microfabricated shock target array technology, any laboratory with a moderate power (0.1 mJ) ultrafast laser system can generate reproducible, well-characterized nanoshock pulses in condensed matter samples at a high repetition rate and probe the shock front dynamics with time resolution of at least a few tens of picoseconds and potentially somewhat better with the new generation of femtosecond lasers. Any solid sample that can be fabricated into a thin layer can be studied without needing to tune the excitation wavelength of the laser, since the shock generation layer has the same absorbance in all arrays. Our anthracene experiments demonstrate how vibrational spectroscopy can be used to determine the shock temperature, pressure, velocity, rise time, and fall time. Although so far we have used only vibrational spectroscopy (CARS) and transient absorption spectroscopy with nanoshocks, it is clear that almost any optical probing method can be used.

With nanoshocks, a great deal of energy can be pumped into a sample in a very short time, in a well-defined manner. When a sample is pumped by a short optical pulse, it is difficult to pump too much energy into the sample in a controlled way, because the optical fields become very large and complicated nonlinear effects including avalanche breakdown occur (sometimes called "femtosecond everythingization"). All these complicated interactions occur in our shock generation layer as well, but the *sample itself* sees only an intense but well-characterized perturbation—a planar front moving at a constant velocity.

Nanoshocks should be regarded as an alternative to optical pumping methods which excite electronic or vibrational degrees of freedom of the sample. The nanoshock pulses produce *large-amplitude mechanical perturbations.* (A typical displacement in our experiments is 15% of the equilibrium intermolecular separation.)

An exciting feature of nanoshocks is the extremely rapid cooling process during nanoshock unloading, which produces cooling rates of hundreds of billions of degrees per second. The mechanism of cooling is the familiar process of adiabatic expansion used in supersonic jet expansions, but it is *far faster* in a solid because the collision frequency is much greater and the sample need expand a tiny amount, only a few percent of initial volume, to produce a large cooling effect. Ultrafast cooling opens up many possibilities for studying molecular materials and biomaterials that are suddenly frozen into metastable configurations not ordinarily observed.

Although much of shock wave physics is presently focused on the problems of studying simple systems such as metals under very high-pressure shock compression, in this article we have tried to illustrate how moderate-pressure nanoshocks could be a powerful tool for ultrafast dynamical studies of complex systems of interest to chemists and biochemists, such as crystalline or amorphous molecular solids, glasses, and biomaterials. Using high repetition rate nanoshocks to study large-

amplitude molecular dynamics in molecular materials important in chemistry and biology is the new wave in shock waves.

Acknowledgment. This research was supported by US Army Research Office Contract DAAH04-96-1-0038, Air Force Office of Scientific Research Contract F49620-97-1-0056, and National Science Foundation Grant DMR 94-04806. We thank Dr. Jeffrey R. Hill of Coe College and Mr. Brent Strickler of UIUC for their work on the myoglobin shock experiment. We thank the referee for insightful comments.

References and Notes

(1) Zel'dovich, Y. B.; Raizer, Y. P. *Physics of Shock Waves and High-Temperature Hydrodynamic Phenomena*; Academic Press: New York, 1966.

(2) Asay, J. R., Shahinpoor, M., Eds. *High-Pressure Shock Compression of Solids*; Springer-Verlag: New York, 1993.

(3) See, e.g.: Schmidt, S., Tao, W. C., Eds. *Shock Compression of Condensed Matter 1995*; American Institute of Physics: New York, 1995; Vol. 370, especially the section on "Optical Studies".

(4) Moore, D. S.; Schmidt, S. C. In *Shock Waves in Condensed Matter 1987*; Schmidt, S. C., Holmes, N. C., Eds.; Elsevier: Amsterdam, 1988; *p* 35. Schmidt, S. C.; Moore, D. S.; Shaner, J. W. *Diagnostics for Determining Phenomenology of Condensed-Phase Shock-Compressed Molecular Systems*; Los Alamos National Laboratory Technical Report LA-UR 83-901, 1993.

(5) Mitchell, A. C.; Nellis, W. J.; Moriarty, J. A.; Heinle, R. A.; Holmes, N. C.; Tipton, R. E.; Repp, G. W. *J. Appl. Phys*. **1991**, *69*, 2981.

(6) Da Silva, L. B.; Celliers, P.; Collins, G. W.; Budil, K. S.; Holmes, N. C.; Barbee, T. W., Jr.; Hammel, B. A.; Kilkenny, J. D.; Wallace, R. J.; Ross, M.; Cauble, R.; Ng, A.; Chiu, G. *Phys. Rev. Lett*. **1997**, *78*, 483.

(7) Harris, P.; Presles, H.-N. *J. Chem. Phys*. **1982**, *77*, 5157.

(8) Leung, K. P.; Doukas, A. G.; Jones, P. H.; Papadimitriou, D.; Alfano, R. R. *Phys. Rev. B* **1985,** *31*, 8329.

(9) White, C. T.; Robertson, D. H.; Elert, M. L. In *Microscopic Simulations of Complex Hydrodynamic Phenomena*; Mareschal, M., Holian, B. L., Eds.; Plenum Press: New York, 1992; p 111.

(10) Celliers, P.; Ng, A.; Xu, G.; Forsman, A. *Phys. Rev. Lett.* **1992**, *68*, 2305.

(11) Sheffield, S. A.; Bloomquist, D. D.; Tarver, C. M. *J. Chem. Phys*. **1984**, *80*, 3831.

(12) See, e.g.: *Ultrafast Phenomena X*; Barbara, P. F., Fujimoto, J. G., Knox, W. H., Zinth, W., Eds.; Springer Ser. Chem. Phys. 62; Springer: Berlin, 1996.

(13) Huston, A. L.; Justus, B. L.; Campillo, A. J. *Chem. Phys. Lett*. **1985**, *118*, 267. Justus, B. L.; Huston, A. L.; Campillo, A. J. *Chem. Phys. Lett*. **1986**, *128*, 274. Justus, B. L.; Merritt, C. D.; Campillo, A. J. *Chem. Phys. Lett*. **1989**, *156*, 64. Lu, X. Z.; Rao, R.; Willman, B.; Lee, S.; Doukas, A. G.; Alfano, R. R. *Phys. Rev. B* **1987**, *35*, 7515. Lu, X. Z.; Garuthara, R.; Lee, S.; Alfano, R. R. *Appl. Phys. Lett*. **1988**, *52*, 93. Garuthara, R.; Lu, X. Z.; Lee, S.; Alfano, R. R. *J. Appl. Phys*. **1988**, *64*, 3737. Lu, X. Z.; Garuthara, R.; Lee, S.; Alfano, R. R. *Appl. Phys. Lett*. **1988**, *52*, 93. Lu, X. Z.; Lee, S.; Garuthara, R.; Alfano, R. R. *Appl. Phys. Lett*. **1987**, *51*, 1789.

(14) Lee, I.-Y. S.; Hill, J. R.; Suzuki, H.; Baer, B. J.; Chronister, E. L.; Dlott, D. D. *J. Chem. Phys.* **1995**, *103*, 8313.

(15) Amiranoff, F.; Fedosejevs, R.; Schmalz, R. F.; Sigel, R.; Teng, Y.-L. *Phys. Rev. A* **1985**, *32*, 3535.

(16) Marsh, S. P., Ed. *LASL Shock Hugoniot Data;* University of California Press: Berkeley, CA, 1980.

(17) Holian, B. L.; Hoover, W. G.; Moran, B.; Straub, G. K. *Phys. Rev. A* **1980**, *22*, 2798.

(18) Cagnoux, J.; Chartagnac, P.; Hereil, P.; Perez, M. *Ann. Phys. Fr*. **1987**, *12*, 451.

(19) Graham, R. A. *Solids Under High-Pressure Shock Compression. Mechanics, Physics and Chemistry*; Springer-Verlag: New York, 1993.

(20) Johnson, J. N.; Barker, L. M. *J. Appl. Phys*. **1969**, *40*, 4321. Swegle, J. W.; Grady, D. E. *J. Appl. Phys*. **1985**, *58*, 692.

(21) Pastine, D. J.; Edwards, D. J.; Jones, H. D.; Richmond, C. T.; Kim, K. In *High-Pressure Science Technology;* Timmerhaus, K. D., Barber, M. S., Eds.; Plenum: New York, 1979; Vol. 2, p 364. Coffey, C. S.; Toton, E. T. *J. Chem. Phys.* **1982**, *76*, 949. Zerilli, F. J.; Toton, E. T. *Phys. Rev. B* **1984**, *29*, 5891. Bardo, R. D. *Int. J. Quantum Chem. Symp.* **1986**, *20*, 455.

(22) Dlott, D. D.; Fayer, M. D. *J. Chem. Phys.* **1990**, *92*, 3798. Tokmakoff, A.; Fayer, M. D.; Dlott, D. D. *J. Phys. Chem*. **1993**, *97*, 1901.

(23) Chen, S.; Tolbert, W. A.; Dlott, D. D. *J. Phys. Chem*. **1994**, *98*, 7759.

(24) Evans, R.; Badger, A. D.; Fallies, F.; Mahdieh, M.; Hall, T. A.; Audebert, P.; Geindre, J.-P.; Gauthier, J.-C.; Mysyrowicz, A.; Grillon, G.; Antonetti, A. *Phys. Rev. Lett*. **1996**, *77*, 3359.

(25) Lee, I.-Y. S.; Hill, J. R.; Dlott, D. D. *J. Appl. Phys*. **1994,** *75*, 4975.

(26) Hambir, S. A.; Franken, J.; Hare, D. E.; Chronister, E. L.; Baer, B. J.; Dlott, D. D. *J. Appl. Phys*. **1997**, *81*, 2157.

(27) Franken, J.; Hambir, S. A.; Hare, D. E.; Dlott, D. D. *Shock Waves* **1997**, *7*, 135.

(28) Tas, G.; Franken, J.; Hambir, S. A.; Dlott, D. D. *Phys. Rev. Lett*. **1997**, *78*, 4585.

(29) Tas, G.; Hambir, S. A.; Franken, J.; Hare, D. E.; Dlott, D. D. *J. Appl. Phys*. **1997**, *82*, 1080.

(30) Trott, W. M.; Renlund, A. M. *J. Phys. Chem*. **1988**, *92*, 5921. Yoo, C. S.; Gupta, Y. M.; Horn, P. D. *Chem. Phys. Lett*. **1989**, *159*, 178. Pangilinan, G. I.; Gupta, Y. M. *J. Phys. Chem*. **1994**, *98*, 4522. Gupta, Y. M.; Pangilinan, G. I.; Winey, J. M.; Constantinou, C. P. *Chem. Phys. Lett*. **1995**, *232*, 341.

(31) Justus, B. L.; Huston, A. L.; Campillo, A. J. *Appl. Phys. Lett*. **1986**, *47*, 1159.

(32) Cottett, F.; Romain, J. P. *Phys. Rev. A* **1982**, *25*, 576. Loeb, A.; Eliezer, S. *Phys. Fluids* **1985**, *28*, 1196.

(33) Kitaigorodsky, A. I. *Molecular Crystals and Molecules;* Academic: New York, 1973.

(34) Vaidya, S. N.; Kennedy, G. C. *J. Chem. Phys*. **1971**, *55*, 987. Nicol, M.; Vernon, M.; Woo, J. T. *J. Chem. Phys.* **1975**, *63*, 1992.

(35) Warnes, R. H. *J. Chem. Phys.* **1970**, *53*, 1088.

(36) Abasbegovic, N.; Vukotic, N.; Colombo, L. J. *Chem. Phys*. **1964**, *41*, 2575.

(37) Schosser, C. L.; Dlott, D. D. *J. Chem. Phys*. **1984**, *80*, 1394.

(38) Eesley, G. L. *Coherent Raman Spectroscopy*; Pergamon: Oxford, 1981.

(39) Hare, D. E.; Dlott, D. D. *Appl. Phys. Lett*. **1994**, *64*, 715.

(40) Califano, S.; Schettino, V.; Neto, N. *Lattice Dynamics of Molecular Crystals;* Springer-Verlag: Berlin, 1981.

(41) Häfner, W.; Kiefer, W. *J. Chem. Phys.* **1987**, *86*, 4582.

(42) Hare, D. E.; Franken, J.; Dlott, D. D. *Chem. Phys. Lett*. **1995**, *244*, 224.

(43) Golub, G. H.; Reinsch, C. *Numer. Math*. **1970**, *14*, 403.

(44) Shrager, R. I.; Hendler, R. W. *Anal. Chem*. **1982**, *54*, 1152. Hofrichter, J.; Sommer, J. H.; Henry, E. R.; Eaton, W. A. *Proc. Natl. Acad. Sci. U.S.A.* **1983**, *80*, 2235.

(45) Franken, J.; Hambir, S. A.; Dlott, D. D. *Mol. Cryst. Liq. Cryst.*, in press.

(46) Hambir, S. A.; Franken, J.; Dlott, D. D. *Rev. High Press. Sci. Technol*., in press.

(47) Chen, S.; Lee, I.-Y. S.; Tolbert, W. A.; Wen, X.; Dlott, D. D. *J. Phys. Chem.* **1992**, *96*, 7178.

(48) Dlott, D. D. In *Laser Spectroscopy of Solids II*; Yen, W., Ed.; Springer-Verlag: Berlin, 1989; p 167.

(49) Chen, S.; Hong, X.; Hill, J. R.; Dlott, D. D. *J. Phys. Chem*. **1995**, *99*, 4525.

(50) Lee, K.-Y.; Gilardi, R. *Mater. Res. Soc. Proc*. **1993**, *296*, 237.

(51) Sorescu, D. C.; Sutton, T. R. L.; Thompson, D. L.; Beardall, D.; Wight, C. A. *J. Mol. Struct.* **1996**, *384*, 87.

(52) Dickerson, R. E.; Geiss, I. *The Structure and Action of Proteins*; Addison-Wesley: New York, 1969.

(53) Antonini, E.; Brunori, M. *Hemoglobin and Myoglobin in Their Reactions with Ligands*; North-Holland: Amsterdam, 1971.

(54) Zipp, A.; Kauzmann, W. *Biochemistry* **1973**, *12*, 4217.

(55) Weber, G.; Drickamer, H. G. *Q. Rev. Biophys*. **1983**, *16*, 89.

(56) Lim, M.; Jackson, T. A.; Anfinrud, P. A. *Proc. Natl. Acad. Sci. U.S.A.* **1993**, *90*, 5801.

(57) Friedman, J. M.; Rousseau, D. L.; Ondrias, M. R. *Annu. Rev. Phys. Chem*. **1982**, *33*, 471.

(58) Ballew, R. M.; Sabelko, J.; Gruebele, M. *Proc. Natl. Acad. Sci. U.S.A.* **1996**, *93*, 5759.